Probing the performance of a Ni-Ca-Ce dual functional material for integrated CO_2 capture and utilization from a synthetic flue gas approximating industrial composition

Lukas C. Buelens[=], Louis Van de Voorde[=], Varun Singh, Hilde Poelman, Guy B. Marin, Vladimir V. Galvita*

Abstract (Executive summary)

Confining CO_2 emissions and accelerating towards a circular carbon economy demand process intensification strategies. This work evaluates integrated CO_2 capture and catalytic conversion over a solid dual functional material in the presence of H_2O and O_2, approximating industrial compositions in a laboratory-scale fixed bed reactor. CO_2 capture from flue gas and its isothermal utilization with H_2 are temporally separated by applying chemical looping with isolated steps driven by CaO and Ni. A ceria-modified dual functional material shows over 60% CO_2 capture efficiency and 70% CO_2 conversion with average space-time yields exceeding 850 kg_{CO_2} $m^{-3}_{reactor}$ h^{-1} and 300 kg_{CO} $m^{-3}_{reactor}$ h^{-1} at 973 K and 120 kPa. Increasing the H_2 feed concentration during the CO_2 utilization step steers the selectivity towards CH_4. The material maintains its performance over 30 cycles using a synthetic flue gas containing CO_2, O_2, and H_2O and 75 mol% H_2 for the CO_2 capture and utilization steps.

Keywords: chemical looping, calcium looping, reverse water-gas shift reaction, methanation, CO_2 utilization

Acknowledgments

L. C. Buelens acknowledges financial support from the Fund for Scientific Research Flanders (FWO Flanders) through a postdoctoral fellowship grant 12E5623N. V. V. Galvita acknowledges a personal grant from the Research Fund of Ghent University (BOF; 01N16319).

Graphical abstract

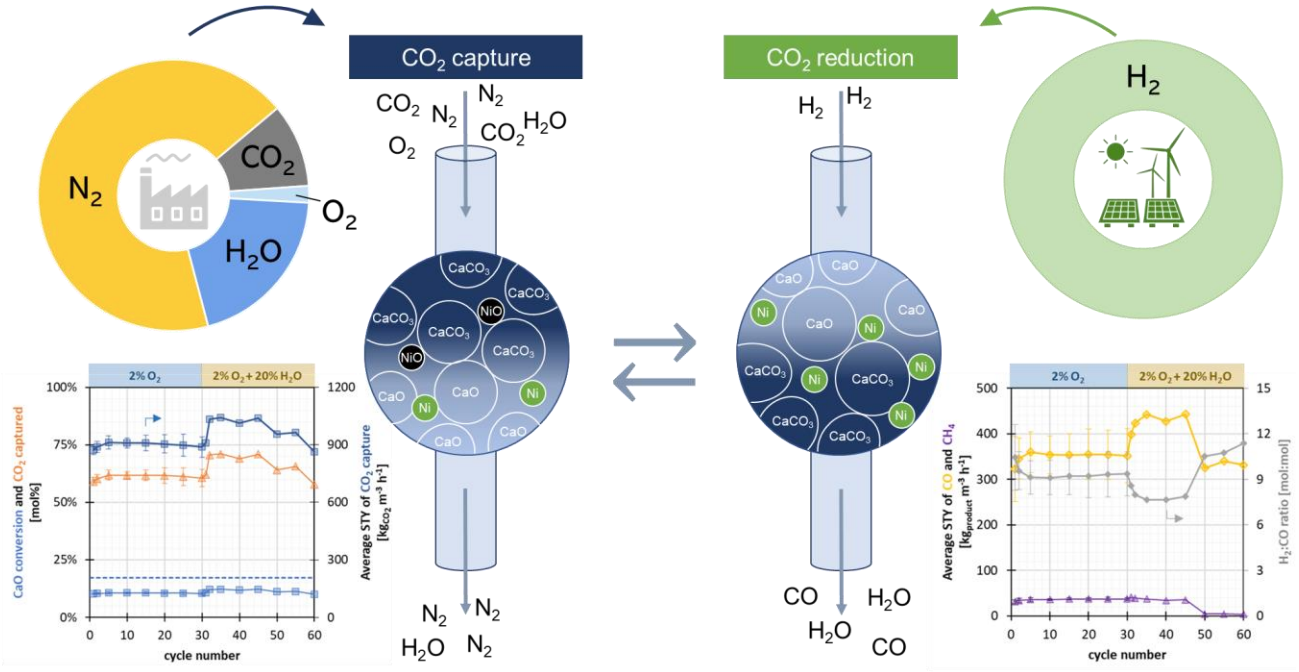

Glossary and list of abbreviations and symbols

Abbreviations

AMU	Atomic mass unit
CaL	Calcium looping
CL-rWGS	Chemical looping mediated reverse water-gas shift reaction
CLC	Chemical looping combustion
DFM	Dual functional material
EDX	Energy dispersive x-ray spectroscopy
GHSV	Gas hourly space velocity in h^{-1}
ICCU	Integrated carbon capture and utilization
MFC	Mass flow controller
MS	Mass spectrometer
NIST	National Institute of Standards and Technology, United States of America
rWGS	Reverse water-gas shift reaction
SEM	Scanning electron microscope
STEM	Scanning transmission electron microscopy
TPR	Temperature-programmed reduction
WHSV	Weight hourly space velocity (g_{feed} g_{DFM} h^{-1})
XRD	X-ray diffraction
STY	Space-time yield
$\overline{STY}$	Average space-time yield

Symbols

$\Delta_r H^0_{298K}$	Standard enthalpy of reaction at 298 K in kJ/mol

Abstract

Confining CO_2 emissions and accelerating towards a circular carbon economy demand process intensification strategies. This work evaluates integrated CO_2 capture and catalytic conversion over a solid dual functional material in the presence of H_2O and O_2, approximating industrial compositions in a laboratory-scale fixed bed reactor. CO_2 capture from flue gas and its isothermal utilization with H_2 are temporally separated by applying chemical looping with isolated steps driven by CaO and Ni. A ceria-modified dual functional material shows over 60% CO_2 capture efficiency and 70% CO_2 conversion with average space-time yields exceeding 850 kg_{CO_2} $m^{-3}_{reactor}$ h^{-1} and 300 kg_{CO} $m^{-3}_{reactor}$ h^{-1} at 973 K and 120 kPa. Increasing the H_2 feed concentration during the CO_2 utilization step steers the selectivity towards CH_4. The material maintains its performance over 30 cycles using a synthetic flue gas containing CO_2, O_2, and H_2O and 75 mol% H_2 for the CO_2 capture and utilization steps.

1. Introduction

Carbon capture and utilization (CCU) aims to capture CO_2 from flue gases or the atmosphere and subsequently convert it into value-added carbonaceous fuels and chemical building blocks[1]. Both processes of capture and conversion rely on adequate materials achieving satisfactory performance and stability. The process efficiency and economic viability of CCU could be enhanced by using dual functional materials (DFMs) in an approach which is commonly termed integrated CO_2 capture and utilization (ICCU), which combines CO_2 capture and conversion in a single process[2]. For the chemical conversion of CO_2, different processes such as methanation, oxidative catalytic alkane dehydrogenation, dry reforming and the reverse water-gas shift reaction (rWGS) have been explored[2]. Although the resulting ICCU processes usually require a high temperature and thus additional energy, they can be run isothermally and continuously by alternating the inlet flow to the reactor. The conventional counterparts of the CO_2 conversion processes require highly concentrated CO_2 to achieve satisfactory average space-time yields ($\overline{STY}$) and practically feasible product separation. In contrast, by combining the capture and conversion of CO_2 over one material in an ICCU process, the direct use of diluted or low-value flue gases (5-15% CO_2) as carbon sources can become viable.

Currently, there is a growing interest in using DFMs that combine calcium looping (CaL) with in situ conversion of released CO_2 during sorbent regeneration. CaL is a chemical looping process based on the reversible carbonation-decarbonation reactions of CaO (equation (1)). The use of CaO has drawn much attention because of its high theoretical CO_2 capacity (0.78 g_{CO_2} per g_{CaO}) and natural abundance. The biggest challenges of CaL are the energy-intensive regeneration[3] and the decrease of chemical reactivity[4] of CaO over multiple cycles.

$$CaCO_3 + CO_2 \rightleftharpoons CaCO_3 \qquad \Delta_r H^0_{298K} = -179\ kJ\ mol^{-1} \qquad (1)$$

At temperatures relevant for CaL (873 – 1173 K), in situ conversion of captured CO_2 improves the kinetics of decarbonation and decreases the decarbonation temperature from 1173 K to around 923 - 1023 K[5]. The lower CaO regeneration temperature and the lower partial pressure of CO_2 during decarbonation decreases sintering of CaO, thereby arresting the decay of its chemical reactivity over multiple cycles[5]. Nevertheless, the decarbonation reaction is highly endothermic (reverse of equation (1)). Considering the typical temperature at which CaO can be regenerated, the two most relevant means to convert captured CO_2

during decarbonation are dry reforming and rWGS, both of which are endothermic reactions. As the former is strongly endothermic (247 kJ mol^{-1}), this work focuses on an ICCU process in which the rWGS (equation (2)) is applied for the combined CaO regeneration and in situ CO_2 conversion. During the catalytic rWGS, CO_2 is reduced by H_2 to CO (equation (2)). A fraction of CO_2 can also be reduced to CH_4 in the presence of excess H_2 via the catalytic methanation reaction (equation (3)).

$$H_2 + CO_2 \rightleftharpoons CO + H_2O \qquad \Delta_r H^0_{298K} = +41\ kJ\ mol^{-1} \qquad (2)$$

$$4H_2 + CO_2 \rightleftharpoons CH_4 + 2H_2O \qquad \Delta_r H^0_{298K} = -165\ kJ\ mol^{-1} \qquad (3)$$

The process concept of cyclic capture and rWGS conversion over a Ni-CaO DFM is illustrated in **Figure 1**, with an approximation of a real flue gas as CO_2-source. In the first step, CO_2 is captured by CaO to form $CaCO_3$. The reducing agent is fed in the second step to release and in situ utilize the captured CO_2 over the present Ni active sites.

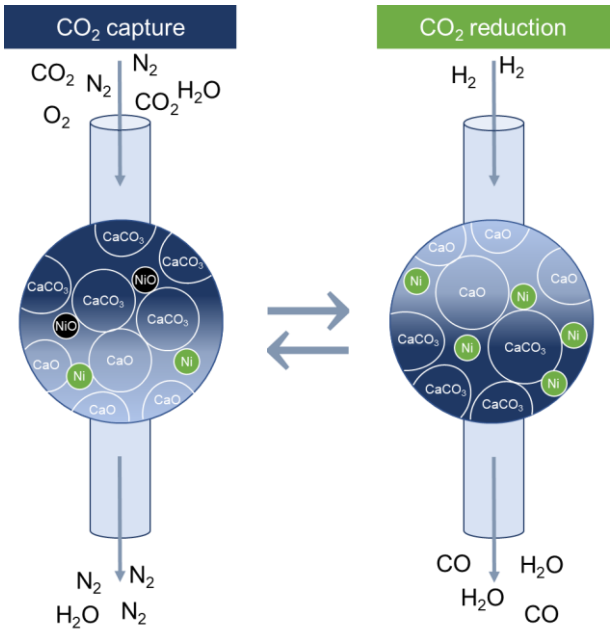

Figure 1. Process schematic for integrated chemical looping CO_2 capture and utilization from flue gases using a dual functional material containing CaO and Ni. In the capture step, CO_2 and residual O_2 in the flue gas are removed by CaO and Ni. In the rWGS step, Ni is regenerated and acts as a catalyst for CO_2 conversion with H_2 into CO, driving the isothermal $CaCO_3$ decomposition through Le Chatelier's principle.

Much of the research work on DFMs for ICCU-rWGS focuses on the application of Ni-CaO systems at operating temperatures ranging from 923 – 1023 K, CO_2 concentrations of 10-15%

and H_2 concentrations of 5, 10 or 100%, while alternative DFM formulations seek to avoid Ni by combining CaO with an Fe-based catalytic function.

Jo et al. studied a Ni/CaO DFM for application in ICCU methanation, DRM and rWGS[6]. During the CO_2 capture step, they used 10% CO_2 and 10% H_2O in inert gas as model flue gas, whereas 10% H_2 in inert was used for the rWGS stage of the ICCU process. Based on thermodynamic and experimental analysis, they proposed 973 K as optimal temperature for the ICCU-rWGS cycle. Wang and co-workers studied the effect of the Ni/CaO synthesis method on their performance as DFMs for ICCU-rWGS[7]. The resulting materials, based on calcium carbide slag as Ca precursor, were tested at 923 K using 10% CO_2 during the CO_2 capture stage and 5% H_2 during the CO_2 utilization stage. Their results show that the DFM synthesized through Ca extraction by propionic acid, followed by filtration and addition of nickel nitrate with citric acid as complexing agent, performed the best in terms of CO_2 uptake and CO yield among the studied materials. The potential synergies in upcycling both gaseous and solid industrial by-products through chemical looping are indeed increasingly appreciated[8]. Another example is the work by S. Sun et al., who investigated the use of marble dust as functional material for ICCU-rWGS at 923 K using 10% CO_2 during the CO_2 capture stage and pure H_2 during the rWGS step[9]. The cheap and abundantly available material was found to exhibit promising rWGS activity, though its CO_2 sorption capacity decreased by 30% over 47 cycles.

H. Sun et al. studied the effect of Ce-modification on $Ca_1Ni_{0.1}$ materials using 15% CO_2 and 5% H_2 in the CO_2 capture and rWGS step of the ICCU process[10]. They found that the modification by ceria resulted in improved CO yields and DFM activity, and hypothesized that CO_2, when released from $CaCO_3$, can directly be reduced over oxygen vacancies generated by ceria owing to its excellent redox properties. Moreover, they found that the thermally resistant ceria could effectively act as a physical barrier to impede material deactivation through CaO and Ni crystallite growth. This can be attributed to the high Tammann temperature[11] of 1337 K for CeO_2, as well as the strong metal-support interaction between Ni and CeO_2[12].

S. Sun et al. studied a range of Ni_xFe_y-CaO materials as DFMs for ICCU-rWGS at 873 – 973 K using 10% CO_2 during the CO_2 capture and 100% H_2 during the rWGS stage[13]. The Ni_1Fe_9-CaO material was found to exhibit the best performance with a CO yield of 11.3 mmol/g_{DFM}, 82.5% CO_2 conversion, and 99.9% CO selectivity at 650°C. In this material, the presence of

$Ca_2Fe_2O_5$ was found to play two major roles, as oxygen carrier for in situ chemical looping CO production and as physical barrier to retard crystallite growth and agglomeration. Shao and coworkers proposed a Fe-Co/Mg-Ca dual functional material and found that the refractory MgO, highly disperse Fe and Co, and hierarchical porous CaO provided a recipe for success in solving the challenge of CaO sintering[14]. This material was found to achieve a CO_2 conversion of 90% and CO selectivity close to 100% when operated at 650°C in an ICCU-rWGS cycle using 10% CO_2 in the CO_2 capture step and pure H_2 in the CO_2 utilization step. Jin et al. proposed a Prussian blue derived Ca-Fe/Zr bifunctional material for a variant of the ICCU-rWGS cycle, in which the bulk of the CO is formed during the CO_2 capture step over reduced Fe[15]. Within their set of sample compositions, they observed that the space-time yield of CO during the CO_2 releasing step increases with the CaO loading, whereas an optimum Fe_2O_3 loading exists for maximizing the CO space-time yield during the CO_2 capture step. In another alternative approach, S. Sun and co-workers studied the application of industrially supplied CaO powder directly as functional material for ICCU-rWGS under 15% CO_2 during carbonation and pure H_2 during the rWGS step of the cycle[16]. Their results show CO_2 conversions in the range of 75 – 90% with a 100% selectivity to CO when operating the process at 873 – 973 K. The CO_2 capture and CO product yields drastically improve as the temperature is increased from 873 K to 973 K at the cost of a more rapid deactivation of the material with a decrease in CO_2 capture capacity from nearly 11 mmol/g_{CaO} to around 3 mmol/g_{CaO} over 50 ICCU cycles.

Indeed, in their 2020 ICCU review, Omodolor et al. highlighted the challenges of cyclic sorbent stability, and suggested that a major challenge for Ni-based DFMs is their deactivation under simulated flue gas conditions (containing oxygen and water) at relatively high operating temperatures (>873 K)[17]. Cu-based systems have been shown to operate well as DFMs for ICCU-rWGS at 623 – 823 K using K/Ba[18] or K/hydrotalcite[19] for the CO_2 sorption functionality. In their study on the FeCrCu/K/MgO-Al_2O_3 DFM, Bobadilla et al. showed that the presence of 5% O_2 and 4% H_2O in a synthetic flue gas (9.5% CO_2 in N_2) resulted in a negative impact on the CO_2 capture efficiency and CO_2 conversion, which was hypothesized to be the result of an altered state of the active sites[19]. As suggested by Lv et al. in their recent perspective article on ICCU, the influence of gas components in actual industrial flue gas on the successive reactions require further investigation[2]. In their 2021 review, S. Sun et al. identified several additional research gaps in the development of ICCU processes, namely engineering aspects such as process design and techno-economic analysis, as well as more fundamental aspects

such as more in-depth understanding of the synergies between the sorbent and catalytic functionality in DFMs[20]. For ICCU-rWGS in particular, they pinpointed a lack of attention of the research community for the H_2:CO ratio of the produced syngas.

The aim of this work is to address and fill in some of the research gaps in ICCU-rWGS as identified over the past years. This study focuses on holistically evaluating the effect of practically relevant operating conditions during both steps of the ICCU cycle by means of four process performance metrics: $\overline{STY}$, product selectivity to CO and CH_4, product purity (H_2:CO ratio), and DFM material utilization. The main operating conditions under consideration in the current study are (1) operating temperature, (2) the hydrogen concentration during the rWGS step of the ICCU cycle, and (3) the presence of O_2 and H_2O during the CO_2 capture step of the ICCU cycle.

2. Experimental

2.1. Material preparation

A simple wet physical mixing method was used to synthesize a DFM with a nominal composition of 40 wt.% NiO, 40 wt.% CaO, and 20 wt.% CeO_2. This DFM has been shown to exhibit excellent stability as DFM for a combined chemical looping process[21]. A mixture of predetermined amounts of calcium d-gluconate monohydrate ($C_{12}H_{22}CaO_{14}\cdot H_2O$, Sigma-Aldrich, 98%), nickel nitrate hexahydrate ($Ni(NO_3)_2\cdot 6H_2O$, Sigma-Aldrich, 99.999%) and cerium nitrate hexahydrate ($Ce(NO_3)_3\cdot 6H_2O$, Sigma-Aldrich, 99.99%) was dissolved in deionized water under continuous stirring at 353 K and the solution was allowed to evaporate under the same conditions. The gel-like remnant was dried overnight at 393 K. The dried solid chunks were crushed and calcined at 1173 K for 1.5 hours after increasing the temperature at 2 K min^{-1} from ambient temperature.

2.2. Material characterization methods

The prepared material was characterized using N_2 sorption at 77 K, scanning electron microscopy with energy dispersive x-ray spectroscopy (SEM-EDX), scanning transmission electron microscopy (STEM), temperature programmed reduction (TPR), and x-ray diffraction (XRD). Further details related to the sample preparation, equipment specifications, and data collection are elaborated in section 1.1. of SI.

2.3. Equilibrium calculations

Equilibrium calculations were performed on the "Equilib" module of FactSage using the FactPS database. For the calculations, temperature, pressure, and the total amount of compounds (CO_2, H_2, and Ar) were provided. An exception was made for calculating the equilibrium CO_2 capture, wherein CO_2 and CaO data were taken from NIST and $CaCO_3$ (calcite) from FactSage. Further details are provided in section 1.2 of SI.

2.4. Cyclic operation testing in a fixed bed reactor

The proposed concept is proven by performing cyclic CO_2 capture and utilization experiments in a quartz fixed-bed reactor with an internal diameter of 7.5 mm, wall thickness of 1 mm, and length of 470 mm. The electrically operated oven of the setup is equipped with three heating zones and four thermocouples. One of these is directly in contact with the solids bed to regulate the temperature accurately. The mass flow controllers (MFCs) (Bronkhorst EL-flow) and a pneumatic valve can rapidly switch the inlet to the reactor, which allows processes with short and alternating cycles. For feeding steam, a Coriolis MFC (Brooks-Coriolis) was used to feed deionized water to an evaporator operating at 453 K. The total inlet gas flow rate was kept constant at $104 \bullet 10^{-6}$ mol s^{-1} (GHSV: 13575 h^{-1}). The inlet lines and valves were heated by heat tracing elements with a temperature set point of 403 K. The outlet of the reactor was connected to a sampling port with an on-line mass spectrometer (MS) (Pfeiffer Vacuum OmniStar QMS 301). The product gases were analyzed by tracking H_2, He, CH_4, H_2O, CO, O_2, Ar, and CO_2 signals at 2 AMU (atomic mass unit), 4 AMU, 15 AMU, 18 AMU, 28 AMU, 32 AMU, 40 AMU, and 44 AMU respectively. Fragmentation patterns were taken into account and Ar, fed continuously at set flowrates, was used as the internal standard. The MS was regularly calibrated with reference gases flowing through an empty reactor at room temperature under the assumption that reactions would not occur either because of very slow kinetics and/or unfavorable thermodynamics. The pressure over the bed was kept constant at approximately 120 kPa by means of a back pressure regulator. The DFMs were pelletized, crushed, and sieved to obtain aggregates in the size range of 355–500 µm before being used in the reactor. The total amount of DFM loaded in the reactor was kept constant at 0.5 g unless mentioned otherwise.

Unless mentioned otherwise, each cycle consisted of 2 steps: CO_2 capture involving carbonation of CaO and CO_2 utilization involving regeneration and rWGS. For the parametric

study to screen process conditions (sections 3.1, 3.2, and 3.3), the following ranges for variations were experimentally tested:

- Temperature: 948 – 1023 K.
- Half-cycle duration for CO_2 capture or carbonation: 120 – 360 seconds.
- Half-cycle duration for CO_2 utilization or regeneration: 36 – 420 seconds.
- H_2 concentration of feed gas during CO_2 utilization or regeneration: 10 – 75 mol%.

A pre-treatment procedure was applied before the screening experiments comprising reduction by 10% H_2 in Ar by ramping the temperature from 473 to 873 K at 10 K min^{-1}, where it was held for 15 min. The temperature was then increased to 1098 K under Ar at 10 K min^{-1} followed by re-oxidation of the DFM by 10% CO_2 for 10 min. A detailed overview of the experiments performed for the parametric study can be found in Table S1 (SI).

For the long-term stability tests at 973 K and 120 kPa, the synthetic flue gas was fed to the reactor for 60 seconds at WHSV = 3.3 g_{CO_2} g_{DFM}^{-1} h^{-1}. Two sets of experiments were performed: dry and wet. In dry conditions, the synthetic flue gas was composed of 10 mol% CO_2, 2 mol% O_2, and Ar (remainder). In wet conditions, the composition matched a typical flue gas stream from a power plant comprising 10 mol% CO_2, 20 mol% H_2O, 2 mol% O_2, and the Ar (remainder). After feeding the synthetic flue gas, 75 mol% H_2 in Ar was fed to the reactor to regenerate the DFM for 40 seconds at WHSV = 1.1 g_{H_2} g_{DFM}^{-1} h^{-1}. The presence of Ar in the regeneration feed gas was necessary for analytical purposes. The pre-treatment procedure before the long-term stability test lasting 60 cycles included: 1) reduction by 75% H_2 in Ar at 998 K for 2 min; 2) gas switch to Ar for 3 min; 3) gas switch to 10% CO_2 in Ar for re-oxidizing the DFM by CO_2 for 1 min; 4) flushing the reactor with Ar for 3 min to fully decarbonate the DFM; 5) reduction by 75% H_2 in Ar for 2 min. The reproducibility tests for the long-term tests comprising 30 cycles under dry conditions were pre-treated with a procedure containing only steps 1 and 2.

A complete list of calculations applied for obtaining the performance metrics for the experiment and the process are detailed in SI section 1.2.

3. Results and discussion

In the following sections, the impact of critical input variables such as operating temperature (section 3.1) and H_2 concentration (section 3.2) in the regeneration gas on the material performance is evaluated. Process performance metrics are discussed in section 3.3

using a compilation of data from experiments designed to screen operating conditions. The full data set of computed values such as conversions, selectivity, average space-time yields, and elemental balances are provided in the SI (Tables S2 to S5). Section 3.4 explores the long-term stability of the material at optimal conditions derived from the screening study and using feed gases approximating realistic industrial compositions. The complete data set of the long-term tests is also provided in Tables S7 to S12.

3.1. Impact of operating temperature

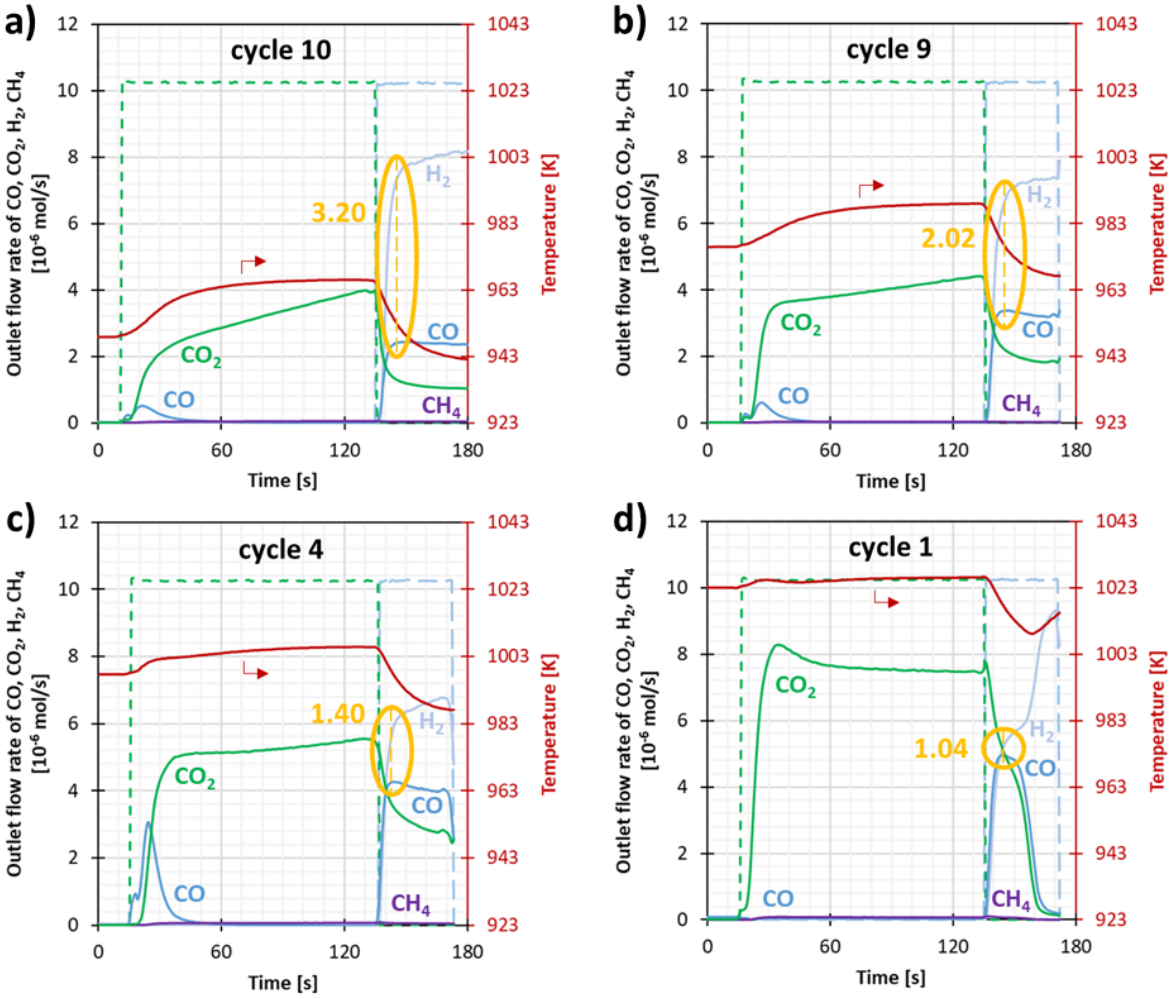

Figure 2. Measured outlet flow rate of gases (CO_2, CO, H_2, CO, and CH_4) in the reactor effluent stream versus time for a single cycle at different temperatures (a – 948 K, b – 973 K, c – 998 K, d – 1023 K). The dashed lines indicate the flow rate of feed gases (green: CO_2 and light blue: H_2) and the yellow ellipsoid indicates the point at which the outlet flow rate of CO is at its maximum. Experimental conditions: CO_2 capture step (1st half-cycle): 10% CO_2 in Ar for 120 seconds and CO_2 utilization step (2nd half-cycle): 10% H_2 in Ar for 36 seconds (except cycle 10, wherein 10% H_2 in Ar was fed for 360 seconds). The catalyst bed consisted of 500 mg DFM.

A lower operating temperature thermodynamically favors CO_2 capture as illustrated in **Figure 2**. As the temperature increases, the fraction of CO_2 *not* captured increases, which is indicated by the decreasing disparity between the measured outlet flow of CO_2 (in green solid line) and the inlet flow of CO_2 (in green dashed line). **Figure 2** a-c show CO production occurring when CO_2 is fed. This may either be attributed to reduction of CeO_2 or carbon deposited in the previous cycle during the regeneration step, which is operated under highly reducing conditions because of the H_2 feed and concomitant CO production. Thermodynamics suggests that carbon formation is unfavorable under the applied conditions. In contrast, reducible oxides such as CeO_2 are well-known to be redox-active and applicable for chemical looping mediated rWGS (CL-rWGS)[22]. Moreover, experimental results from other researchers have also reported CO production during the CO_2 capture step when the DFM comprised reducible oxides such as ceria[23] or iron oxides[13, 15]. Based on the above reasoning, it is assumed that CO production in the CO_2 capture step can be solely attributed to ceria in the DFM acting as the solid mediator for CL-rWGS. The absence of CO in **Figure 2**d, which shows the first experiment of the campaign (Table S1), corroborates this hypothesis.

The exothermic nature of the carbonation reaction is highlighted by the accompanying increase in temperature consistently observed in **Figure 2** a-d when CO_2 is fed to the DFM. This increase diminishes at higher temperatures because the total amount of CO_2 captured or reacting decreases as dictated by the thermodynamics of CaO carbonation. During the CO_2 utilization step when H_2 is fed, the formation of CO at all studied temperatures is accompanied by a sharp temperature decrease reflecting the endothermic nature of both rWGS and $CaCO_3$ decarbonation. CO_2 and CO formation persist over the 36 seconds of the CO_2 utilization step, indicating incomplete decarbonation of $CaCO_3$ in the DFM at 948 K, 973 K, and 998 K over the applied step duration. Faster kinetics of $CaCO_3$ decarbonation coupled with lower CO_2 captured at 1023 K explain the full regeneration of the DFM at this temperature. Despite the faster kinetics at elevated temperatures, the rate of decarbonation remains rate-limiting during the CO_2 utilization step as suggested by the reaction quotient (Figure S1). Further analysis of the reaction quotients indicates that the rWGS reaction is close to equilibrium, in contrast to the decarbonation reaction.

Like carbonation and decarbonation, rWGS is a reversible reaction, the kinetics and thermodynamics of which are favored at higher temperatures. Thus, higher temperatures improve H_2 and CO_2 conversion, thereby decreasing the H_2:CO ratio. For the sake of

estimating the best-case scenario for CO_2 conversion and the ability of the catalyst to hasten the approach to equilibrium, the point at which maximum production of CO is observed is highlighted with a yellow ellipsoid in **Figure 2** a-d. This point is used to compute the lowest H_2:CO ratio observed during the transient operation of the CO_2 utilization step. **Figure 3**a shows how the minimum H_2:CO ratio (yellow open circles on the secondary y-axis) becomes lower at higher temperature, thereby alluding to the thermodynamics at play.

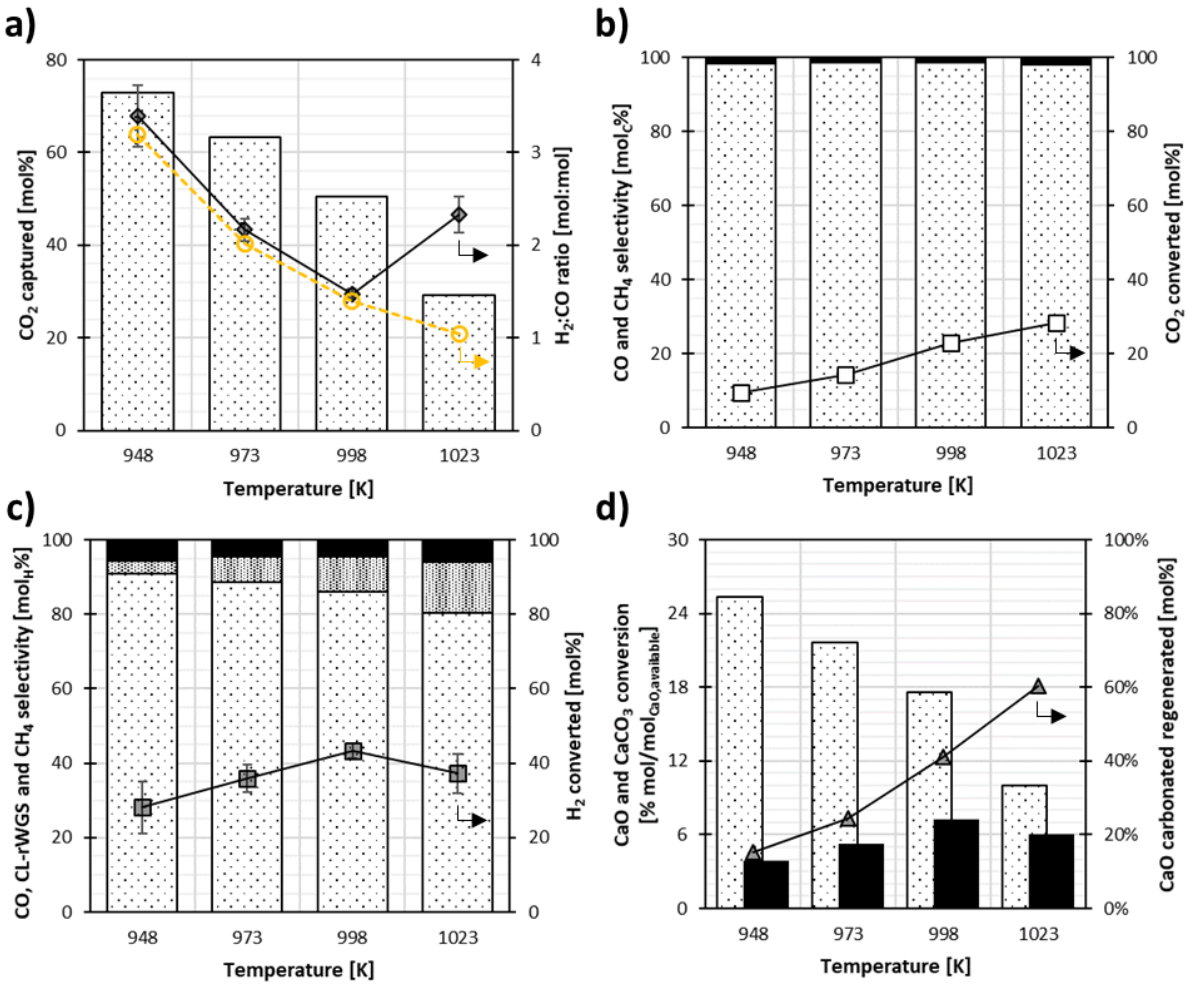

Figure 3. Impact of temperature on a) CO_2 captured (▭) and the H_2:CO ratio of the product gas (◆ cumulative values; ◆ at the point of maximum CO production rate); b) CO_2 conversion (□) and the selectivity of CO_2 conversion (▭ CO selectivity; ▬ CH_4 selectivity); c) H_2 conversion (■) and the selectivity of H_2 conversion (▭ selectivity to H_2O associated with CO product; ▩ selectivity to H_2O associated with ceria reduction; ▬ selectivity to H_2O and CH_4 associated with CH_4 product); d) utilization of the CO_2 sorption capacity of CaO (▭ CaO conversion), CO_2 releasing capacity of formed $CaCO_3$ (▬ $CaCO_3$ conversion) and CaO regeneration (▲ CaO carbonated regenerated). Experimental conditions: CO_2 capture step (1st half-cycle): 10% CO_2 in Ar for 120 seconds and CO_2 utilization step (2nd half-cycle): 10% H_2 in Ar for 36 seconds (except cycle 10, wherein 10% H_2 in Ar was

fed for 360 seconds. Error bars wherever displayed indicate the spread of the values when the same metric is calculated via two or more different methods (see section 1.2 of SI for more details).

Figure 3b shows that the CO_2 conversion increases with temperature (secondary y-axis). Methanation is not favored at high temperatures and less than 2% of CO_2 converted results in CH_4 formation. **Figure 3**c shows the analogous form of **Figure 3**b with H_2 conversion and selectivity of H_2 instead of CO_2. Given the high value of H_2[24], its efficient utilization in this process is critical. Increasing the temperature from 948 K to 998 K increases the H_2 conversion from 28% to 43%, which can be attributed to the higher thermodynamic driving force for rWGS. Apart from that, higher temperature also improves the reduction of CeO_2 by H_2, thereby increasing its contribution for CL-rWGS, i.e. the use of fed H_2 for CO production during the subsequent CO_2 capture step. The cumulative H_2 conversion drops from 43% to 37% when the temperature is further increased from 998 K to 1023 K. This can be attributed to CO_2 becoming a limiting reactant at 1023 K during the CO_2 utilization step (**Figure 2**d), which is a direct consequence of the limited amount of CO_2 captured at 1023 K in the preceding CO_2 capture step (dotted bars on the primary y-axis **Figure 3**a). This effect is also reflected in the trend breaking high cumulative H_2:CO ratio of the product gas at 1023 K in **Figure 3**a (black open diamonds on the secondary y-axis).

Figure 3d shows the impact of temperature on the regeneration of the CO_2 sorbent. At lower temperature, a large disparity exists between the CO_2 captured in the CO_2 capture step (dotted bars) and the CO_2 released and/or converted during the CO_2 utilization step (black bars). Although the kinetics of decarbonation are strongly improved via Le Chatelier's principle when released CO_2 is quickly converted into CO[16], the evaluated temperatures in this study remain low enough to hamper the decarbonation reaction. Moreover, equilibrium limitations are also imposed by rWGS, which prohibits complete conversion of CO_2 and fed H_2 into CO and H_2O. An increase in temperature significantly improves the kinetics of decarbonation and provides a higher thermodynamic driving force for CO_2 conversion resulting in lower disparity between the CO_2 captured and released in the two half-cycles. The secondary y-axis on the plot (**Figure 3**d) shows the percentage of CaO carbonated during the CO_2 capture step which is regenerated during the CO_2 utilization step, thereby providing an advanced visual cue to the above discussion. It should be noted that the utilization of the sorbent at all studied temperatures remained relatively low at less than 25%. Several researchers active in the field of calcium looping have noted that carbonation occurs in two

steps: 1) a fast kinetic regime limited to the surface and sub-surface and 2) a slow diffusion-controlled regime[25]. By limiting the utilization rate of CaO to lower values, the process can be operated in the so-called "fast kinetic regime". However, this comes at the cost of having a larger reactor with under-utilized material, which impacts the average space-time yield. A trade-off between the material utilization in the bed and the reaction kinetics associated with it can inform an optimization study to maximize the average space-time yield.

3.2. Impact of H_2 concentration on selectivity and regeneration duration

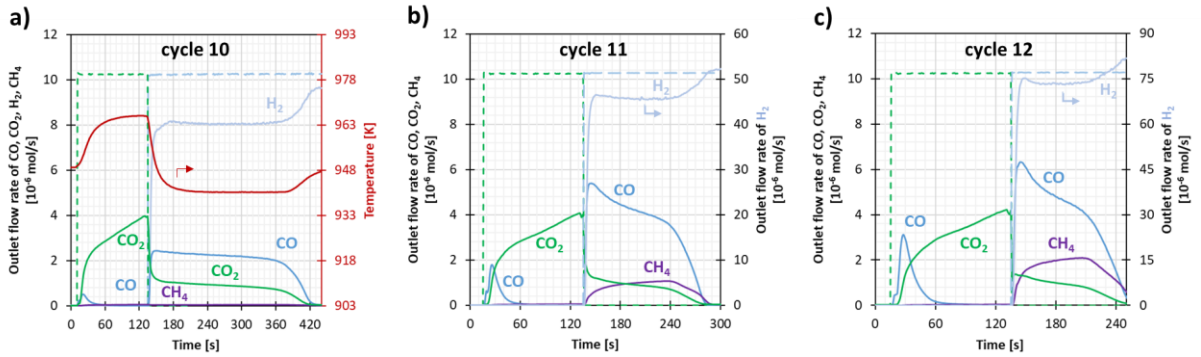

Figure 4. Measured outlet flow rate of gases (CO_2, CO, H_2, CO, and CH_4) in the reactor effluent stream against time for a single cycle with different concentrations of H_2 fed in the CO_2 utilization step (a – 10 mol% H_2, b – 50 mol% H_2, and c – 75 mol% H_2). CO_2 capture step (1st half-cycle): 10% CO_2 in Ar for 120 seconds and CO_2 utilization step (2nd half-cycle): 10 - 75% H_2 in Ar with duration adapted based on observed CO and CO_2 outlet. The furnace temperature was controlled at 948 K for all cycles. The catalyst bed consisted of 500 mg DFM. Temperature profiles for b) and c) are presented in Figure S2.

Figure 4 illustrates the following effects of increasing the H_2 concentration during the CO_2 utilization step on the process: 1) the duration of the CO_2 utilization step decreases by a factor of 2-3 with increasing H_2 concentration, 2) the H_2:CO ratio increases by a factor of 3 – 5, and 3) the production of methane becomes favorable at higher H_2 concentrations driven by larger thermodynamic forces. It should be noted that these cycles were performed at a fixed duration of the CO_2 capture step, while the duration of the CO_2 utilization step was adaptively shortened when no more carbonaceous products were measured by the MS.

The CO_2 captured (**Figure 5**a) decreases slightly with increasing H_2 concentration in the feed gas used for the CO_2 utilization step although the operating temperature and pressure, carbonation duration, and the CO_2 content in the flue gas feed are kept constant. This may be attributed to either material deactivation or analytical errors introduced by significantly changing the concentration of Ar, the internal standard for the MS, in the regeneration gas.

The secondary y-axis of **Figure 5**a depicts the cumulative H_2:CO ratio (black open diamonds) and the H_2:CO ratio at the point of highest CO production during the CO_2 utilization step (yellow open circles) of the product stream. Such high H_2:CO ratios can severely impair further utilization of the product stream given the fact that commodity chemicals such as methanol require H_2:CO ratio only slightly greater than 2. When CO_2 is present, the optimal H_2:CO_2 ratio lies between 1 and 3[26]. It should be noted that these experiments were performed at a relatively low temperature of 948 K to maximize the CO_2 capture efficiency (more than 70%), which – as evidenced in the above discussion – also results in a higher H_2:CO product ratio.

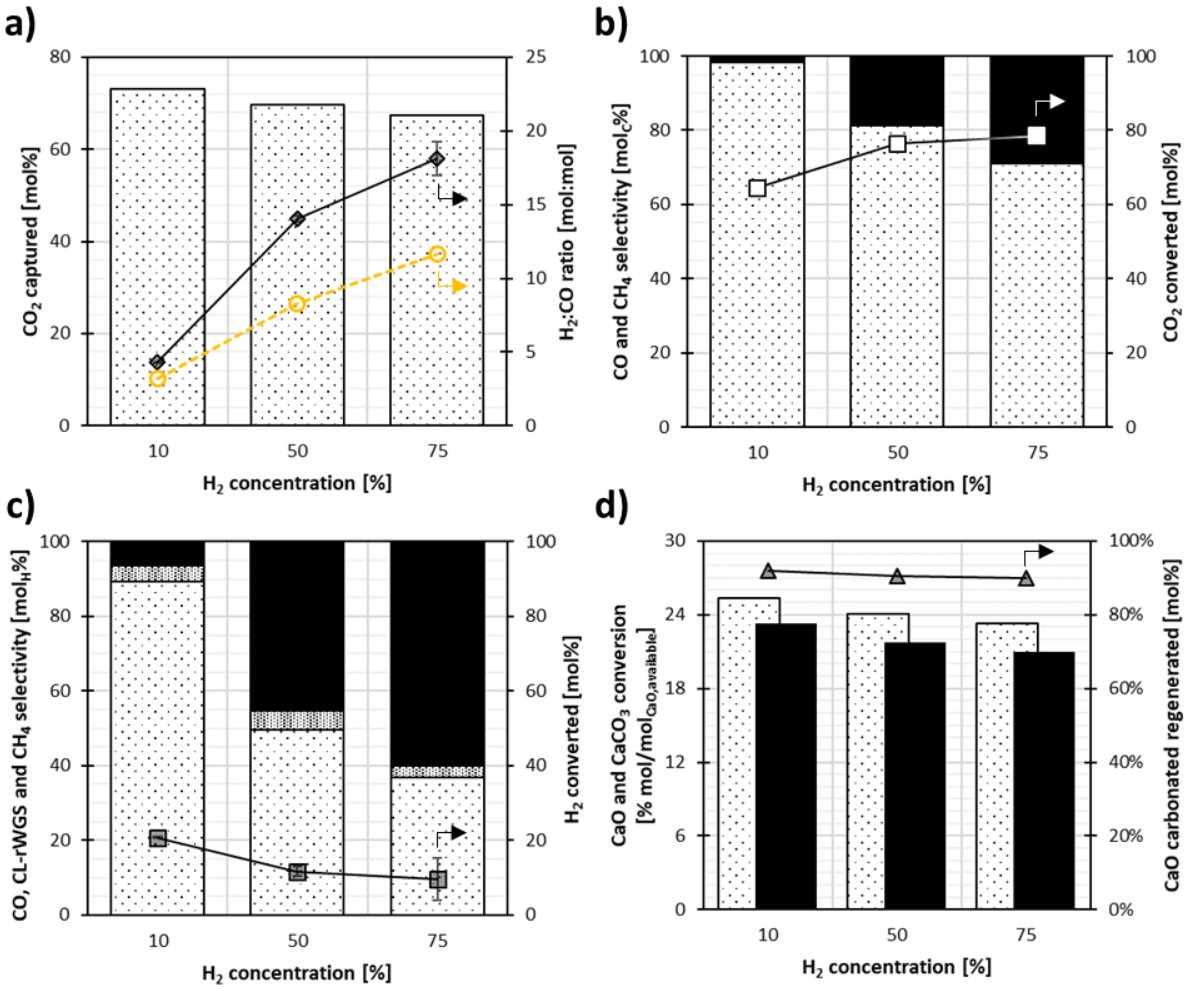

Figure 5. Impact of H_2 concentration on a) CO_2 captured (▭) and the H_2:CO ratio of the product gas (-◆- cumulative values; -○- at the point of maximum CO production rate); b) CO_2 conversion (-□-) and the selectivity of CO_2 conversion (▭ CO selectivity; ▬ CH_4 selectivity); c) H_2 conversion (-▬-) and the selectivity of H_2 conversion (▭ selectivity to H_2O associated with CO product; ▩ selectivity to H_2O associated with ceria reduction; ▬ selectivity to H_2O and CH_4 associated with CH_4 product); d) utilization of the CO_2 sorption capacity of CaO (▭ CaO conversion), CO_2 releasing capacity of

formed $CaCO_3$ (▬ $CaCO_3$ conversion) and CaO regeneration (-▲- CaO carbonated regenerated). Experimental conditions: CO_2 capture step (1st half-cycle): 10% CO_2 in Ar for 120 seconds and H_2 utilization step (2nd half-cycle): 10 - 75% H_2 in Ar with duration adapted based on observed CO and CO_2 outlet. The furnace temperature was controlled at 948 K for all cycles. Error bars wherever displayed indicate the spread of the values when the same metric is calculated via two or more different methods (see section 1.2 of SI for more details).

The combination of higher H_2 concentration in the regeneration gas fed in the CO_2 utilization step and a low temperature of 948 K increases the selectivity of CO_2 conversion to methane. Both factors indeed favor the thermodynamics of methanation, an exothermic reaction favored at high reactant pressure[27]. Both the CO_2 conversion (white squares on secondary y-axis of **Figure 5**b) and H_2 conversion (grey squares on secondary y-axis of **Figure 5**c) increase when the H_2 concentration of the feed gas used in the CO_2 utilization step increases from 10 mol% to 50 mol%. A further increase in H_2 concentration from 50 mol% to 75 mol% has little impact on CO_2 and H_2 conversions. This can be attributed to the released CO_2 becoming the limiting reactant and excess H_2 being fed during the regeneration when 75 mol% H_2 is fed. Interestingly, an increase in H_2 concentration of the regeneration gas strongly impacts the selectivity of CO_2 and H_2 conversion to CH_4. Almost 60% of the converted H_2 is consumed for CH_4 formation when the H_2 concentration of the regeneration gas is 75 mol%, reflecting the increased thermodynamic driving force for methanation at high partial pressure of H_2 and the significant catalytic activity of the DFM towards methanation.

The experiments discussed in this sub-section were performed under conditions designed to ensure complete decarbonation of $CaCO_3$, thereby fully regenerating the material. Thus, **Figure 5**d shows that the total amount of $CaCO_3$ decarbonated during the CO_2 utilization step is close to the amount of CaO carbonated in the CO_2 capture step. More than 90% of CaO carbonated was decarbonated eventually leaving only a small discrepancy between the two. The physical phenomena underlying this discrepancy could be accumulation of $CaCO_3$ and/or a deviation in the carbon balance caused by the limited accuracy of the analytical instrument (MS).

3.3. Evaluation of process and material performance metrics

Figure 6 displays a compilation of experimental data points obtained by varying process conditions such as duration of the CO_2 capture and CO_2 utilization step, operating temperature, and H_2 concentration. **Figure 6** a-e all show that under the probed operating

conditions, the reaction kinetics are rapid enough to approach equilibrium under most of the probed conditions. **Figure 6**a shows that only in some cases the measured H_2:CO ratio is lower than its equilibrium value. This may be attributed to utilization of H_2 for the reduction of CeO_2, which is not accounted for in the equilibrium calculations (see section 1.2 of SI for details). Other values of H_2:CO ratio which are higher than the equilibrium value represent cases when equilibrium is not reached either due to excess H_2 fed or slower kinetics. **Figure 6**b displays that, for most experiments, the actual CO_2 capture is lower than the equilibrium CO_2 capture. FactSage predicted no CO_2 capture at 1023 K, 120 kPa total pressure, and 10 mol% CO_2 feed, which were conditions used in 25% of the screening experiments. Thus, data were partly used from NIST (CaO and CO_2), which supported CO_2 capture at above conditions consistent with the experimental findings. It should be noted that this calculation does not consider the fed CO_2 that is lost as CO, thereby overestimating the equilibrium CO_2 capture value. As the thermodynamically computed value is purely a function of temperature (see section 1.2 of SI for more details), traversing the x-axis of **Figure 6**b from left to right is indicative of decreasing temperature.

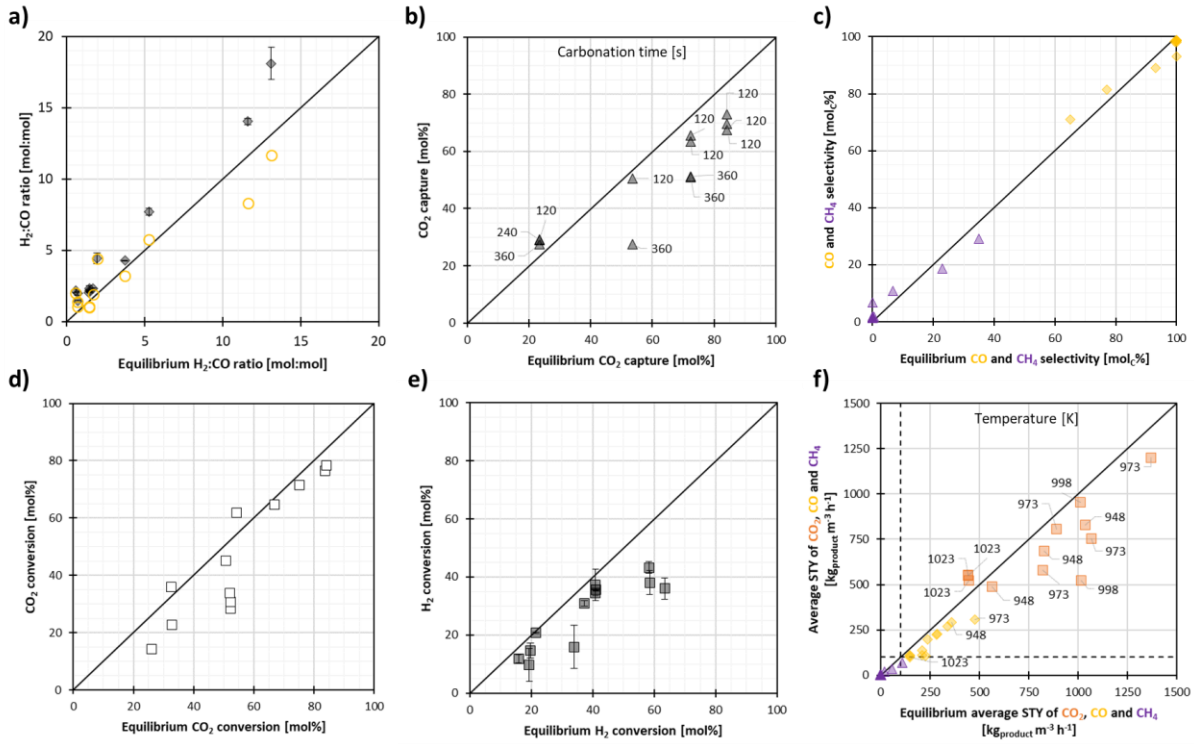

Figure 6. Experimental vs thermodynamic equilibrium-based a) H_2:CO ratio (◆ cumulative experimental values; ○ experimental value at the point of maximum CO production rate), b) CO_2 capture, c) selectivity of CO_2 conversion to CO (◆) and CH_4 (▲), d) CO_2 conversion, e) H_2 conversion,

and f) average space-time yield (▫ CO_2; ◇ CO; △ CH_4). Annotations in b) and f) indicate the duration of the CO_2 capture step, i.e. the 1st half-cycle, and the operating temperature of the cycle for which the average space-time yields are presented. Dashed lines in f) indicate the typical minimum average space-time yield (also termed reactor productivity) for industrial reactors as reported by Lange[28]. Error bars wherever displayed indicate the spread of the values when the same metric is calculated via two or more different methods (see section 1.2 of SI for more details).

The lack of data points at high equilibrium H_2 conversion (>70%) in **Figure 6**e is indicative of the trade-offs involved in operating ICCU isothermally. High equilibrium H_2 conversion requires high temperature and/or excess CO_2. On the one hand, high temperature isothermal operation results in lack of captured CO_2 in the 1st half-cycle to react with H_2 in the subsequent half-cycle. On the other hand, excess CO_2 can be provided by isothermally operating at lower temperature. However, low temperature operation hampers rWGS, thereby limiting H_2 conversion. As previously reported for a similar chemical looping CO_2 utilization process by Singh et al.[29], a trade-off should be found between improved production rates and product purity typically achieved using a temperature-swing, and irreversible efficiency losses associated with repeated heating and cooling. In contrast, isothermal fixed bed operation induces less strain on the functional material associated with repeated temperature swings and can be operated with a higher thermal efficiency[30]. A detailed analysis of this trade-off is however beyond the scope of this work.

Figure 6f shows that, considering the entire cycle duration, the CO_2 capture $\overline{STY}$ is in the range of 400 to 1300 kg $m^{-3}_{reactor}$ h^{-1} for the probed window of experimental conditions. These values are in the same order of magnitude as an absorption based CO_2 scrubber for post-combustion capture[31] and orders of magnitude higher than CO_2 capture from air[32]. The highest CO_2 capture $\overline{STY}$ and CO $\overline{STY}$ were achieved at 973 K. **Figure 7** compares the CO_2 utilization rate (y-axis) to the CO_2 capture rate (x-axis) with the diagonal representing 100% utilization of CO_2 captured. At 973 K, the best CO $\overline{STY}$ (~300 kg $m^{-3}_{reactor}$ h^{-1}) is reached at a high CO_2 capture $\overline{STY}$ of around 750 kg $m^{-3}_{reactor}$ h^{-1}. Since this temperature provides the best trade-off between the rate of CO_2 capture and CO production, it is chosen for the long-term stability tests discussed in the following section. At lower temperatures, the discrepancy between CO_2 capture and CO $\overline{STY}$ becomes larger owing to less favorable rWGS and more

favorable CO_2 capture thermodynamics, whereas at higher temperatures, CO $\overline{STY}$ becomes limited by the much lower CO_2 capture $\overline{STY}$.

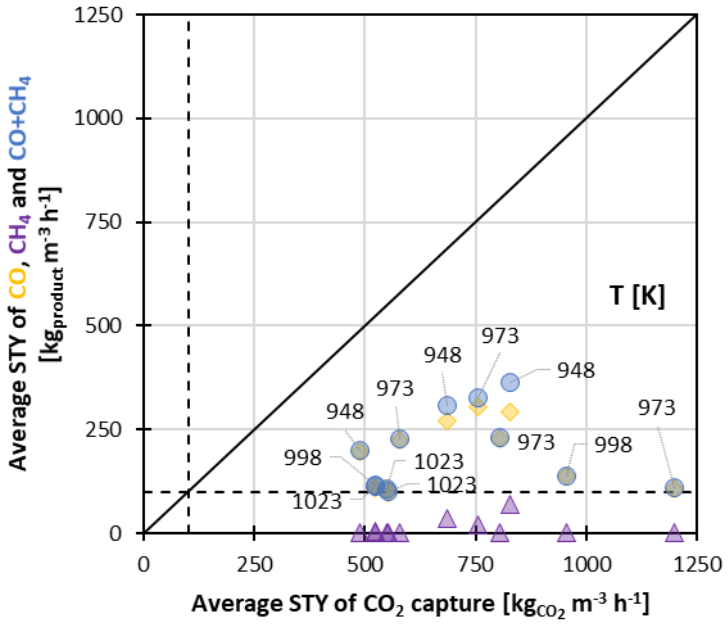

Figure 7. Average space-time yield of CO_2 utilization (◇ CO; △ CH_4; ○ $CO+CH_4$) as a function of average space-time yield of CO_2 capture. Dashed lines indicate the typical minimum average space-time yield (also termed reactor productivity) for industrial reactors as reported by Lange[28].

3.4. Impact of synthetic flue gas containing O_2 and H_2O on cyclic stability

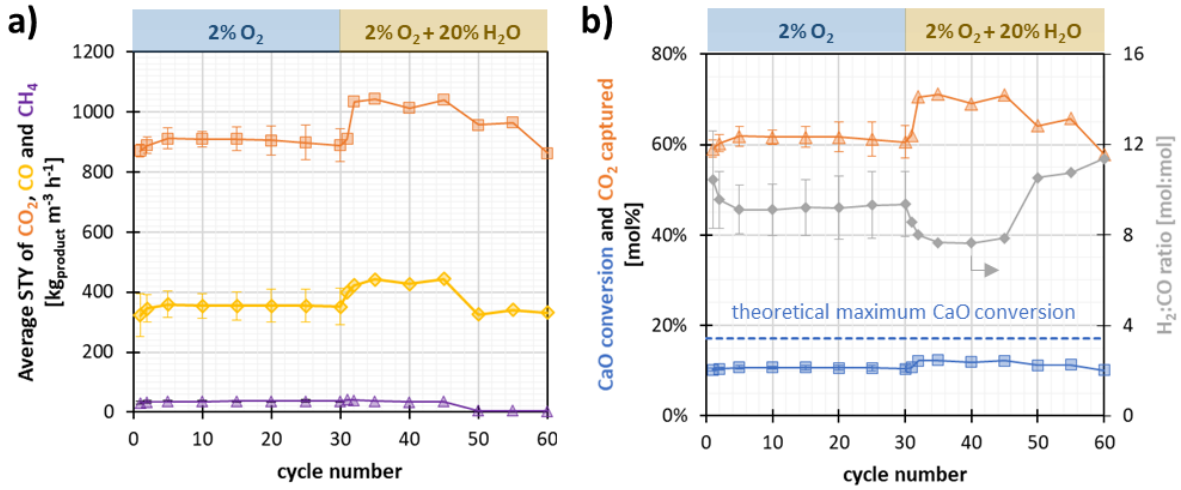

Figure 8. Stability tests over 60 ICCU-rWGS cycles, out of which the first 30 cycles include O_2 (denoted: dry cycles) and the next 30 cycles include O_2 and H_2O (denoted: wet cycles) in the synthetic flue gas. a) Average space-time yield of CO_2 capture (-□-), CO (-◇-) and CH_4 (-△-) over 60 cycles. b) CaO conversion (-□-), CO_2 captured (-△-) and H_2:CO ratio (-◇-) over 60 cycles. The horizontal dashed

line (---) indicates the theoretical maximum CaO conversion, i.e. at 100% CO_2 captured, when taking into consideration the experimental conditions. The stability tests were performed at 973 K and 120 kPa. CO_2 capture step: 10 mol% CO_2, 2 mol% O_2, (20 mol% H_2O) in Ar (remainder). CO_2 utilization step: 75% H_2 in Ar. Note that the error bars over the first 30 cycles are generated from a set of 3 independent repeat experiments.

Figure 8a shows that the $\overline{STY}$ of CO_2 capture, CO, and CH_4 remain fairly stable and close to 900, 350, and 30 kg $m^{-3}_{reactor}$ h^{-1} over the 30 dry cycles (1 – 30), indicating more than 40% mass-based conversion (>70 mol%) of captured CO_2. The complete datasets are presented in Tables S7 to S12 (SI section 3). When steam is added from cycle 31 onwards, the $\overline{STY}$ of CO_2 and CO increase while that of CH_4 remains constant until cycle 45. A steep drop in all three average space-time yields is observed thereafter. This decline is attributed to accumulation of H_2O (raw data displayed in Figure S3b, SI section 3) and further confirmed by the absence of outlet CH_4, the formation of which would be strongly disfavored by the presence of excess H_2O. The presence of excess H_2O also impairs the accuracy of the MS, which results in poor carbon balances over the last 10 cycles (cfr. e1 in Table S11, SI section 3). Nevertheless, it is worth noting that the $\overline{STY}$ of CO_2 and CO in the final wet cycle are near to identical to those in the first dry cycle of the experimental run. Apart from that, all the O_2 fed during these cycles was captured by reduced Ni, while the impact on the CL-rWGS contribution seems minimal (cfr. Table S8, SI section 3). The resulting effect of O_2 capture by Ni is a strong contribution to the process of CLC driven by H_2 and mediated by Ni/NiO redox pair, wherein NiO is reduced to Ni by H_2 fed during the CO_2 utilization step and re-oxidized by O_2 fed during the subsequent CO_2 capture step. The oxidation of Ni is highly exothermic and would hence preferably be coupled with the endothermic decarbonation reaction[33]. On the other hand, industrial flue gases are typically available at low temperatures, meaning that Ni oxidation by O_2 present in the flue gas could assist in preheating the flue gas to operating temperatures relevant for CO_2 capture temperature[34]. Indeed, the contrasting heat management requirements for the two half-cycles of this process do provide opportunities for innovative conceptual and engineering solutions. Examples of conceptual solutions include auto-thermal operation by tuning the feed gas[35], combining endothermic and exothermic reactions[34, 36] and using an appropriate metal oxide catalyst[37]. Engineering solutions include decreasing the energy consumption using heat integration via pinch analysis[38] and multi-variable optimization[39], improving exergy efficiency[38, 40], reactor design[41], and optimizing the reactor operating conditions.

Figure 8b shows that the CO_2 captured over the 30 dry cycles remains above 60%. A slight decrease in CO_2 captured is accompanied by a small and gradual increase in the carbon balance in the early cycles (1 to 10) (Table S11, SI section 3). This may be attributed to $CaCO_3$ accumulation (Figure S4c). Co-feeding H_2O from cycle 31 onwards improves the CO_2 captured, which indicates the beneficial impact of steam addition during carbonation on the reactivity of CaO as previously reported[42], given that mild carbonation conditions of temperature and CO_2 concentration are applied[43].

The H_2:CO ratio of the product gas remains stable between 9 and 10 during the dry cycles and decreases further to a value between 7 and 9 during the initial wet cycles. The H_2O accumulation after cycle 45 described earlier affects the H_2:CO ratio negatively by hampering H_2 conversion through the rWGS and methanation reaction. CaO utilization, which expresses the amount of CaO utilized with respect to the amount of CaO placed in the reactor, reaches 10-12% throughout the run. The theoretical maximum CaO utilization of 17% is based on the CO_2 fed to the reactor and assuming complete (100%) CO_2 capture. Characterization data of the DFM comparing its fresh and after long-term stability tests via N_2 sorption, H_2-TPR, XRD, and STEM-EDX along with SEM-EDX data for compositional analysis of the as prepared material are provided in section 4 of the SI.

4. Conclusions

A dual functional material (DFM) comprising 40 wt.% NiO, 40wt.% CaO and 20wt.% CeO_2 was prepared using a simple wet physical mixing method for an integrated CO_2 capture and utilization process. Reactor tests proved that the selected DFM effectively utilizes 1) the CO_2 sorption capability of CaO to capture CO_2 from a diluted CO_2 stream in one step and 2) the catalytic activity of Ni to convert the captured CO_2 with fed H_2 in the subsequent CO_2 conversion and regeneration step.

For industrial operation of such a process, the H_2 feedstock during the regeneration step should be of a high purity to avoid complex and costly downstream separation. The experimental results of this work indicate that the concentration of H_2 in the regeneration gas has a significant impact on the selectivity of CO_2 conversion to either CH_4 or CO. The increased selectivity to CH_4 at higher H_2 concentrations, which closely approximates a realistic regeneration gas, is remarkable given the high operating temperature (~973 K) and low total pressure (~120 kPa). The average space-time yield of CO was most promising at 973 K

reaching more than 300 kg_{CO} $m_{reactor}^{-3}$ h^{-1}. Hence, 973 K was chosen as the temperature at which long-term stability of the material was further investigated. These experiments were performed by executing 30 cycles using synthetic feed gases, i.e. a gas containing 10% mol CO_2 and 2 mol% O_2 during the CO_2 capture step and 75 mol% H_2 during the CO_2 conversion and regeneration step. The reproducible experiments verified that the DFM did not undergo deactivation over the course of these cycles. 30 additional cycles were executed by adding steam (20 mol%) to the synthetic CO_2-containing flue gas along with O_2. These experiments further confirmed that the DFM withstands the presence of steam and even improves its performance to some extent. The cyclic process maintained a CO_2 capture $\overline{STY}$ and CO $\overline{STY}$ of more than 850 kg_{CO_2} $m_{reactor}^{-3}$ h^{-1} and 300 kg_{CO} $m_{reactor}^{-3}$ h^{-1} while producing a stream with an H_2:CO ratio between 7 and 12.

This work shows that Ni-Ca-Ce DFMs are promising materials for integrated CO_2 capture and conversion processes exhibiting enhanced stability under operating conditions which include the presence of O_2 and H_2O in the CO_2-containing flue gas and concentrated H_2 feed for utilizing the captured CO_2. Although relatively low, the observed selectivity of CO_2 conversion to CH_4 is undesirable because it consumes valuable H_2 and adds further complexity to the downstream separation and utilization of the product syngas stream. Future efforts towards tuning the selectivity of CO_2 conversion, further reducing the H_2:CO ratio, improving the efficiency of H_2 utilization, and analyzing engineering solutions for heat management will pave the way to commercial deployment of this technology.

Bibliography

(1) Buelens, L. C.; Poelman, H.; Marin, G. B.; Galvita, V. V. 110th Anniversary: Carbon Dioxide and Chemical Looping: Current Research Trends. *Ind Eng Chem Res* **2019**, *58* (36), 16235-16257. DOI: 10.1021/acs.iecr.9b02521.
(2) Lv, Z.; Chen, S.; Huang, X.; Qin, C. Recent progress and perspective on integrated CO_2 capture and utilization. *Curr. Opin. Green Sustain. Chem.* **2023**, *40*, 100771. DOI: 10.1016/j.cogsc.2023.100771.
(3) Rodriguez, N.; Alonso, M.; Grasa, G.; Abanades, J. C. Heat requirements in a calciner of $CaCO_3$ integrated in a CO_2 capture system using CaO. *Chemical Engineering Journal* **2008**, *138* (1), 148-154. DOI: 10.1016/j.cej.2007.06.005.
(4) Kierzkowska Agnieszka, M.; Pacciani, R.; Müller Christoph, R. CaO-Based CO_2 Sorbents: From Fundamentals to the Development of New, Highly Effective Materials. *ChemSusChem* **2013**, *6* (7), 1130-1148. DOI: 10.1002/cssc.201300178.
(5) Han, R.; Wang, Y.; Xing, S.; Pang, C.; Hao, Y.; Song, C.; Liu, Q. Progress in reducing calcination reaction temperature of Calcium-Looping CO_2 capture technology: A critical review. *Chemical Engineering Journal* **2022**, *450*, 137952. DOI: 10.1016/j.cej.2022.137952.
(6) Jo, S. B.; Woo, J. H.; Lee, J. H.; Kim, T. Y.; Kang, H. I.; Lee, S. C.; Kim, J. C. CO_2 green technologies in CO_2 capture and direct utilization processes: methanation, reverse water-gas shift, and dry reforming of methane. *Sustainable Energy & Fuels* **2020**, *4* (11), 5543-5549. DOI: 10.1039/D0SE00951B.
(7) Wang, G.; Guo, Y.; Yu, J.; Liu, F.; Sun, J.; Wang, X.; Wang, T.; Zhao, C. Ni-CaO dual function materials prepared by different synthetic modes for integrated CO_2 capture and conversion. *Chemical Engineering Journal* **2022**, *428*, 132110. DOI: 10.1016/j.cej.2021.132110.
(8) Singh, V.; Buelens, L. C.; Poelman, H.; Marin, G. B.; Galvita, V. V. Chemical looping: a technology platform for upcycling low-grade industrial resources. *Discover Chemical Engineering* **2023**, *3* (1), 12. DOI: 10.1007/s43938-023-00028-3.
(9) Sun, S.; Wang, Y.; Zhao, X.; Zhang, C.; Wu, C. One step upcycling CO_2 from flue gas into CO using natural stone in an integrated CO_2 capture and utilisation system. *Carbon Capture Science & Technology* **2022**, *5*, 100078. DOI: 10.1016/j.ccst.2022.100078.
(10) Sun, H.; Wang, J.; Zhao, J.; Shen, B.; Shi, J.; Huang, J.; Wu, C. Dual functional catalytic materials of Ni over Ce-modified CaO sorbents for integrated CO_2 capture and conversion. *Applied Catalysis B: Environmental* **2019**, *244*, 63-75. DOI: 10.1016/j.apcatb.2018.11.040.
(11) Moulijn, J. A.; van Diepen, A. E.; Kapteijn, F. Catalyst deactivation: is it predictable?: What to do? *Applied Catalysis A: General* **2001**, *212* (1), 3-16. DOI: 10.1016/S0926-860X(00)00842-5.
(12) Du, X.; Zhang, D.; Shi, L.; Gao, R.; Zhang, J. Morphology Dependence of Catalytic Properties of Ni/CeO_2 Nanostructures for Carbon Dioxide Reforming of Methane. *The Journal of Physical Chemistry C* **2012**, *116* (18), 10009-10016. DOI: 10.1021/jp300543r.
(13) Sun, S.; He, S.; Wu, C. Ni promoted Fe-CaO dual functional materials for calcium chemical dual looping. *Chemical Engineering Journal* **2022**, *441*, 135752. DOI: 10.1016/j.cej.2022.135752.
(14) Shao, B.; Hu, G.; Alkebsi, K. A. M.; Ye, G.; Lin, X.; Du, W.; Hu, J.; Wang, M.; Liu, H.; Qian, F. Heterojunction-redox catalysts of $Fe_xCo_yMg_{10}CaO$ for high-temperature CO_2 capture and in situ conversion in the context of green manufacturing. *Energy & Environmental Science* **2021**, *14* (4), 2291-2301. DOI: 10.1039/D0EE03320K.

(15) Jin, B.; Ouyang, T.; Zhang, Z.; Zhao, Y.; Zhang, H.; Yao, W.; Huang, G.; Liang, Z. Prussian blue derived Ca-Fe bifunctional materials for chemical looping CO_2 capture and in-situ conversion. *Separation and Purification Technology* **2023**, *320*, 123975. DOI: 10.1016/j.seppur.2023.123975.
(16) Sun, S.; Lv, Z.; Qiao, Y.; Qin, C.; Xu, S.; Wu, C. Integrated CO_2 capture and utilization with CaO-alone for high purity syngas production. *Carbon Capture Science & Technology* **2021**, *1*, 100001. DOI: 10.1016/j.ccst.2021.100001.
(17) Omodolor, I. S.; Otor, H. O.; Andonegui, J. A.; Allen, B. J.; Alba-Rubio, A. C. Dual-Function Materials for CO_2 Capture and Conversion: A Review. *Ind Eng Chem Res* **2020**, *59* (40), 17612-17631. DOI: 10.1021/acs.iecr.0c02218.
(18) Hyakutake, T.; van Beek, W.; Urakawa, A. Unravelling the nature, evolution and spatial gradients of active species and active sites in the catalyst bed of unpromoted and K/Ba-promoted Cu/Al_2O_3 during CO_2 capture-reduction. *Journal of Materials Chemistry A* **2016**, *4* (18), 6878-6885. DOI: 10.1039/C5TA09461E.
(19) Bobadilla, L. F.; Riesco-García, J. M.; Penelás-Pérez, G.; Urakawa, A. Enabling continuous capture and catalytic conversion of flue gas CO_2 to syngas in one process. *Journal of CO_2 Utilization* **2016**, *14*, 106-111. DOI: /10.1016/j.jcou.2016.04.003.
(20) Sun, S.; Sun, H.; Williams, P. T.; Wu, C. Recent advances in integrated CO_2 capture and utilization: a review. *Sustainable Energy & Fuels* **2021**, *5* (18), 4546-4559. DOI: 10.1039/D1SE00797A.
(21) Singh, V.; Buelens, L. C.; Poelman, H.; Saeys, M.; Marin, G. B.; Galvita, V. V. Intensifying blue hydrogen production by in situ CO_2 utilisation. *Journal of CO2 Utilization* **2022**, *61*, 102014. DOI: 10.1016/j.jcou.2022.102014.
(22) Galvita, V. V.; Poelman, H.; Bliznuk, V.; Detavernier, C.; Marin, G. B. CeO_2-Modified Fe_2O_3 for CO_2 Utilization via Chemical Looping. *Ind Eng Chem Res* **2013**, *52* (25), 8416-8426. DOI: 10.1021/ie4003574.
(23) Wu, J.; Zheng, Y.; Fu, J.; Guo, Y.; Yu, J.; Chu, J.; Huang, P.; Zhao, C. Synthetic Ni–CaO–CeO_2 dual function materials for integrated CO_2 capture and conversion via reverse water–gas shift reaction. *Separation and Purification Technology* **2023**, *317*, 123916. DOI: 10.1016/j.seppur.2023.123916.
(24) Do, T. N.; You, C.; Kim, J. A CO_2 utilization framework for liquid fuels and chemical production: techno-economic and environmental analysis. *Energy & Environmental Science* **2022**, *15* (1), 169-184. DOI: 10.1039/D1EE01444G.
(25) Scaltsoyiannes, A.; Antzaras, A.; Koilaridis, G.; Lemonidou, A. Towards a generalized carbonation kinetic model for CaO-based materials using a modified random pore model. *Chemical Engineering Journal* **2021**, *407*. DOI: 10.1016/j.cej.2020.127207.
(26) Dieterich, V.; Buttler, A.; Hanel, A.; Spliethoff, H.; Fendt, S. Power-to-liquid via synthesis of methanol, DME or Fischer–Tropsch-fuels: a review. *Energy & Environmental Science* **2020**, *13* (10), 3207-3252. DOI: 10.1039/d0ee01187h.
(27) Strucks, P.; Failing, L.; Kaluza, S. A Short Review on Ni-Catalyzed Methanation of CO_2: Reaction Mechanism, Catalyst Deactivation, Dynamic Operation. *Chemie Ingenieur Technik* **2021**, *93* (10), 1526-1536. DOI: 10.1002/cite.202100049.
(28) Lange, J.-P. Fuels and Chemicals Manufacturing; Guidelines for Understanding and Minimizing the Production Costs. *CATTECH* **2001**, *5* (2), 82-95. DOI: 10.1023/A:1011944622328.

(29) Singh, V.; Buelens, L. C.; Poelman, H.; Saeys, M.; Marin, G. B.; Galvita, V. V. Carbon monoxide production using a steel mill gas in a combined chemical looping process. *Journal of Energy Chemistry* **2022**, *68*, 811-825. DOI: 10.1016/j.jechem.2021.12.042.
(30) Muhich, C. L.; Evanko, B. W.; Weston, K. C.; Lichty, P.; Liang, X.; Martinek, J.; Musgrave, C. B.; Weimer, A. W. Efficient Generation of H_2 by Splitting Water with an Isothermal Redox Cycle. *Science* **2013**, *341* (6145), 540-542. DOI: 10.1126/science.1239454.
(31) Zanco, S. E.; Pérez-Calvo, J.-F.; Gasós, A.; Cordiano, B.; Becattini, V.; Mazzotti, M. Postcombustion CO_2 Capture: A Comparative Techno-Economic Assessment of Three Technologies Using a Solvent, an Adsorbent, and a Membrane. *ACS Engineering Au* **2021**, *1* (1), 50-72. DOI: 10.1021/acsengineeringau.1c00002.
(32) Sabatino, F.; Grimm, A.; Gallucci, F.; van Sint Annaland, M.; Kramer, G. J.; Gazzani, M. A comparative energy and costs assessment and optimization for direct air capture technologies. *Joule* **2021**, *5* (8), 2047-2076. DOI: 10.1016/j.joule.2021.05.023.
(33) Singh, V.; Buelens, L. C.; Poelman, H.; Saeys, M.; Marin, G. B.; Galvita, V. V. Decarbonisation of steel mill gases in an energy-neutral chemical looping process. *Energy Conversion and Management* **2022**, *254*, 115248. DOI: 10.1016/j.enconman.2022.115248.
(34) Galvita, V. V.; Poelman, H.; Marin, G. B. Combined Chemical Looping: New Possibilities for Energy Storage and Conversion. *Energ Fuel* **2017**, *31* (10), 11509-11514. DOI: 10.1021/acs.energyfuels.7b02490.
(35) Hu, J.; Buelens, L.; Theofanidis, S.-A.; Galvita, V. V.; Poelman, H.; Marin, G. B. CO_2 conversion to CO by auto-thermal catalyst-assisted chemical looping. *Journal of CO_2 Utilization* **2016**, *16*, 8-16. DOI: 10.1016/j.jcou.2016.05.006.
(36) Tian, S.; Li, K.; Jiang, J.; Chen, X.; Yan, F. CO_2 abatement from the iron and steel industry using a combined Ca–Fe chemical loop. *Appl Energ* **2016**, *170*, 345-352. DOI: 10.1016/j.apenergy.2016.02.120.
(37) Abanades, J. C.; Murillo, R.; Fernandez, J. R.; Grasa, G.; Martinez, I. New CO_2 Capture Process for Hydrogen Production Combining Ca and Cu Chemical Loops. *Environ. Sci. Technol.* **2010**, *44* (17), 6901-6904, Article. DOI: 10.1021/es101707t.
(38) Jin, B.; Zhao, Y.; Fan, Y.; Deng, Z.; Liang, Z. Thermal management for chemical looping systems with chemical production. *Chem Eng Sci* **2020**, *214*, 115431. DOI: 10.1016/j.ces.2019.115431.
(39) Deng, Z.; Jin, B.; Zhao, Y.; Gao, H.; Huang, Y.; Luo, X.; Liang, Z. Process simulation and thermodynamic evaluation for chemical looping air separation using fluidized bed reactors. *Energy Conversion and Management* **2018**, *160*, 289-301. DOI: 10.1016/j.enconman.2018.01.039.
(40) Ishida, M.; Zheng, D.; Akehata, T. Evaluation of a chemical-looping-combustion power-generation system by graphic exergy analysis. *Energy* **1987**, *12* (2), 147-154. DOI: 10.1016/0360-5442(87)90119-8.
(41) Adanez, J.; Abad, A.; Garcia-Labiano, F.; Gayan, P.; de Diego, L. F. Progress in Chemical-Looping Combustion and Reforming technologies. *Progress in Energy and Combustion Science* **2012**, *38* (2), 215-282. DOI: 10.1016/j.pecs.2011.09.001.
(42) Donat, F.; Florin, N. H.; Anthony, E. J.; Fennell, P. S. Influence of High-Temperature Steam on the Reactivity of CaO Sorbent for CO_2 Capture. *Environ. Sci. Technol.* **2012**, *46* (2), 1262-1269. DOI: 10.1021/es202679w.
(43) Arcenegui Troya, J. J.; Moreno, V.; Sanchez-Jiménez, P. E.; Perejón, A.; Valverde, J. M.; Pérez-Maqueda, L. A. Effect of Steam Injection during Carbonation on the Multicyclic Performance of Limestone ($CaCO_3$) under Different Calcium Looping Conditions: A

Comparative Study. *ACS Sustainable Chemistry & Engineering* **2022**, *10* (2), 850-859. DOI: 10.1021/acssuschemeng.1c06314.